J|A|C|S
ARTICLES
Published on Web 03/11/2004

Structure Distribution in an Elastin-Mimetic Peptide $(VPGVG)_3$ Investigated by Solid-State NMR

X. L. Yao and M. Hong*

Contribution from the Department of Chemistry, Iowa State University, Ames, Iowa 50011

Received June 14, 2003; E-mail: mhong@iastate.edu

Abstract: Elastin is an extracellular-matrix protein that imparts elasticity to tissues. We have used solid-state NMR to determine a number of distances and torsion angles in an elastin-mimetic peptide, $(VPGVG)_3$, to understand the structural basis of elasticity. C−H and C−N distances between the V6 carbonyl and the V9 amide segment were measured using $^{13}C-^{15}N$ and $^{13}C-^{1}H$ rotational-echo double-resonance experiments. The results indicate the coexistence of two types of intramolecular distances: a third of the molecules have short C−H and C−N distances of 3.3 ± 0.2 and 4.3 ± 0.2 Å, respectively, while the rest have longer distances of about 7 Å. Complementing the distance constraints, we measured the (ϕ, ψ) torsion angles of the central pentameric unit using dipolar correlation NMR. The ψ-angles of P7 and G8 are predominantly ~150°, thus restricting the majority of the peptide to be extended. Combining all torsion angles measured for the five residues, the G8 Cα chemical shift, and the V6−V9 distances, we obtained a bimodal structure distribution for the PG residues in VPGVG. The minor form is a compact structure with a V6−V9 C═O−H^N hydrogen bond and can be either a type II β-turn or a previously unidentified turn with Pro ($\phi = -70°$, $\psi = 20 \pm 20°$) and Gly ($\phi = -100 \pm 20°$, $\psi = -20 \pm 20°$). The major form is an extended and distorted β-strand without a V6−V9 hydrogen bond and differs from the ideal parallel and antiparallel β-strands. The other three residues in the VPGVG unit mainly adopt antiparallel β-sheet torsion angles. Since $(VPGVG)_3$ has the same ^{13}C and ^{15}N isotropic and anisotropic chemical shifts as the elastin-mimetic protein $(VPGXG)_n$ (X = V and K, $n = 195$), the observed conformational distribution around Pro and Gly sheds light on the molecular mechanism of elastin elasticity.

Introduction

Mature elastin is a highly cross-linked extracellular-matrix protein that is responsible for the elasticity of many connective tissues, blood vessels, lungs, and skins of vertebrates.[1] The protein contains two alternating domains. The hydrophobic domain consists of repetitions of short peptide units rich in Gly, Ala, Val, and Pro and is responsible for the elasticity of the protein. Between the hydrophobic domains are Ala and Lys-rich hydrophilic domains that cross-link the polypeptide chains through the Lys residues. While it is known that entropy plays an important role in elastin elasticity, the structural basis of elasticity still remains controversial due to the amorphous nature of the protein. Two schools of theory have been proposed. The first postulates that elastin contains kinetically free and unstructured chains similar to rubber.[2−4] The second class of theory proposes that the hydrophobic part of the protein consists of structured domains of either globular or fibrillar shapes, and the protein is able to return to its original conformation after stretching.[5,6] While global conformational information on natural and recombinant elastin was gleaned from infrared spectroscopy and circular dichroism,[7,8] higher-resolution structural information came from studies of synthetic peptides mimicking the elastin sequence. One common repeat sequence is VPGVG. On the basis of molecular modeling, X-ray diffraction, and solution NMR of the cyclic peptide c-$(VPGVG)_3$, Urry and co-workers proposed that the VPGVG unit adopts a type II β-turn structure around the Pro-Gly pair.[9−11] Repetition of this β-turn gives rise to a right-handed helix termed β-spiral. The elastomeric driving force is believed to result from reduced librational entropy of the VGV segments linking the β-turns when the protein is stretched.[12,13] A different repeat unit, GXGGX, has also been studied and found to consist of a mixture of turn structures and extended structures.[1,14,15] Similarly, the elastomeric restoring force is believed to result from reduced chain mobility as the protein is stretched.

(1) Debelle, L.; Tamburro, A. M. *Int. J. Biochem. Cell Biol.* **1999**, *31*, 261−272.
(2) Hoeve, C. A. J.; Flory, P. J. *Biopolymers* **1974**, *13*, 677−686.
(3) Hoeve, C. A. J.; Flory, P. J. *J. Am. Chem. Soc.* **1958**, *80*, 6523−6526.
(4) Aaron, B. B.; Gosline, J. M. *Nature* **1980**, *287*, 865−867.
(5) Weis-Fogh, T.; Anderson, S. O. *Nature* **1970**, *227*, 718−721.
(6) Gary, W. R.; Sandberg, L. B.; Foster, J. A. *Nature* **1973**, *246*, 461−466.
(7) Debelle, L.; Alix, A. J.; Jacob, M. P.; Huvenne, J. P.; Berjot, M.; Sombret, B.; Legrand, P. *J. Biol. Chem.* **1995**, *270*, 26099−26103.
(8) Debelle, L.; Alix, A. J.; Wei, S. M.; Jacob, M. P.; Huvenne, J. P.; Berjot, M.; Legrand, P. *Eur. J. Biochem.* **1998**, *258*, 533−539.
(9) Venkatachalam, C. M.; Urry, D. W. *Macromolecules* **1981**, *14*, 1225−1229.
(10) Urry, D. W.; Chang, D. K.; Krishna, N. R.; Huang, D. H.; Trapane, T. L.; Prasad, K. U. *Biopolymers* **1989**, *28*, 819−833.
(11) Cook, W. J.; Einspahr, H.; Trapane, T. L.; Urry, D. W.; Bugg, C. E. *J. Am. Chem. Soc.* **1980**, *102*, 5502−5505.
(12) Urry, D. W. *J. Protein Chem.* **1988**, *7*, 1−34.
(13) Urry, D. W. *J. Protein Chem.* **1988**, *7*, 81−114.
(14) Castiglione-Morelli, A.; Scopa, A.; Tamburro, A. M.; Guantieri, V. *Int. J. Biol. Macromol.* **1990**, *12*, 363−368.
(15) Lelj, F.; Tamburro, A. M.; Villani, V.; Grimaldi, P.; Guantieri, V. *Biopolymers* **1992**, *32*, 161−172.

To date, few high-resolution structural studies have been carried out directly on elastin and linear elastin-mimetic peptides in the solid state, due to the insoluble and noncrystalline nature of the protein. Solid-state NMR is a powerful tool for investigating the structure of such disordered systems and can play an important role in elucidating elastin structure and dynamics.[16−18] Using ^{13}C and ^{15}N chemical shifts, we have recently investigated the secondary structure of an elastin-mimetic recombinant protein, $[(VPGVG)_4(VPGKG)]_{39}$.[19] Our analysis supports the type II β-turn structure at Pro-Gly, but rejects ideal α-helical, β-sheet, and type I β-turn structures. Moreover, the protein exhibits significant conformational heterogeneity, manifested as broad line widths of the ^{13}C and ^{15}N spectra. However, more detailed information on the nature of this conformational heterogeneity is difficult to obtain from chemical shifts, because the shift difference between various conformations is often small compared to the line width. For example, the Gly Cα sheet-helix isotropic shift difference is only ∼2 ppm, and its turn-sheet separation is at most 1 ppm.[20−22] Thus, measurement of direct structural parameters such as internuclear distances and torsion angles would be highly desirable for understanding elastin conformational heterogeneity. Our previous study was conducted on a ^{13}C selectively and extensively labeled recombinant protein,[23] where spectral overlap and the lack of labeling of most carbonyl carbons prevented the measurement of precise internuclear distances and torsion angles. Therefore, in this work, we use a site-specific labeled synthetic peptide, $(VPGVG)_3$, to obtain information on the conformation of the long-chain protein. Earlier work has established that short VPGVG peptides exhibit similar properties such as inverse-temperature transition as elastin-mimetic proteins.[24] We show that the 15-residue $(VPGVG)_3$ is a good model system for the long-chain $[(VPGVG)_4(VPGKG)]_{39}$, since it exhibits nearly identical ^{13}C and ^{15}N chemical shifts as the protein. We have determined a number of distances, torsion angles, and conformation-dependent chemical shifts in $(VPGVG)_3$. The results reveal that the PG residues in the VPGVG repeat sequence adopt a combination of tight turn and distorted β-strand structures. Thus, it appears that the elastic function is built into the amino acid sequence of the protein as two types of minimum-energy conformers, one compact and the other extended, and a shift in the conformational equilibrium distinguishes the extended and the relaxed states.

Materials and Methods

Materials. A series of specifically ^{13}C- and ^{15}N-labeled $(VPGVG)_3$ peptides were synthesized by solid-phase peptide synthesis. ^{13}C- and ^{15}N-labeled FMOC amino acids were obtained from Cambridge Isotope Laboratories (Andover, MA) and Spectra Stable Isotopes (Columbia, MD). All ^{13}C and ^{15}N labels were placed in the central pentameric unit of the peptide to minimize the influence of possible structural disorder at the two ends of the molecule. For the distance experiments, the V6 carbonyl carbon and the V9 nitrogen were labeled, and the sample was designated V6V9. For ψ-angle measurements, the backbone ^{15}N, $^{13}C\alpha$, and ^{13}CO sites of the first residue and the ^{15}N of the second residue were labeled. We used V6P7 to designate backbone ^{13}C and ^{15}N labeling at V6 and ^{15}N labeling at P7. Peptides G8V9, V9G10, and G10V11 have similar meanings. Due to the lack of backbone-only labeled Pro, the P7G8 sample contained ^{13}C and ^{15}N uniformly labeled Pro. The unlabeled protein $[(VPGVG)_4(VPGKG)]_{39}$, termed poly(Lys-25), was a gift from Professor Conticello (Emory University). A typical 4-mm MAS rotor contained about 20−40 mg of lyophilized sample.

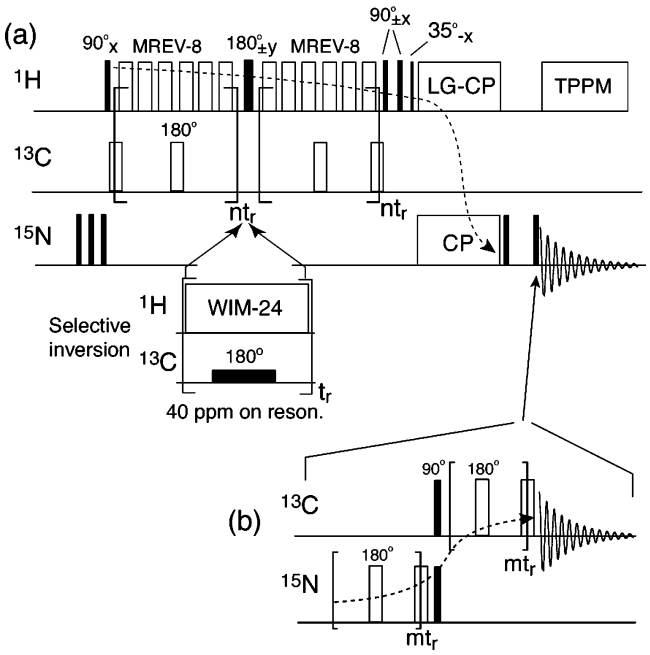

Figure 1. Pulse sequence for the C−H REDOR experiment. (a) After ^{1}H excitation, rotor-synchronized 180° pulses are applied on the ^{13}C and ^{1}H channels to reintroduce the C−H dipolar coupling, while H−H homonuclear interaction is averaged by MREV-8. Contribution of the natural abundance aliphatic carbons to C−H dephasing is removed by a selective ^{13}C 180° pulse on resonance with the aliphatic carbons while ^{1}H evolution is suspended by a WIM sequence. A short LG-CP step transfers the H^N magnetization to its directly bonded ^{15}N for detection. (b) Addition of a $^{15}N-^{13}C$ TEDOR pulse train allows ^{13}C detection of the C−H REDOR signal. This filters out the signals of molecules with long C−N distances, allowing selective detection of molecules with short C−N distances.

NMR Experiments. The NMR experiments were conducted on a Bruker DSX-400 spectrometer (Karlsruhe, Germany) at 9.4 T (100.70 MHz for ^{13}C and 40.58 MHz for ^{15}N), using a 4-mm triple-resonance MAS probe. Typical radio frequency (rf) field strengths for the ^{1}H channel were 70 kHz for decoupling and 50 kHz for cross polarization (CP). Carbon and nitrogen 90° pulse lengths were typically 5 and 6 μs, respectively. All experiments were conducted at 293 ± 2 K.

$^{13}C-^{1}H$ and $^{13}C-^{15}N$ Distance Measurements. A newly developed $^{13}C-^{1}H$ rotational echo double resonance (REDOR) experiment (Figure 1a) was used to measure the distance between V6 CO and V9 H^N.[25] The ^{1}H magnetization evolved under the recoupled $^{13}C-^{1}H$ dipolar interaction for 2n rotor periods. All except for the central 180° pulse was applied on the ^{13}C channel. Meanwhile, a MREV-8 sequence[26] was applied on the ^{1}H channel to suppress the $^{1}H-^{1}H$ homonuclear coupling. Inserted into the middle of the C−H REDOR period was one rotor period containing a soft ^{13}C 180° pulse centered at 40 ppm. This soft 180° pulse selectively inverted the aliphatic carbon polariza-

(16) Perry, A.; Stypa, M. P.; Tenn, B. K.; Kumashiro, K. K. *Biophys. J.* **2002**, *82*, 1086−1095.
(17) Yao, X. L.; Conticello, V. P.; Hong, M. *Magn. Reson. Chem.*, in press.
(18) Fleming, W. W.; Sullivan, C. E.; Torchia, D. A. *Biopolymers* **1980**, *19*, 597−617.
(19) Hong, M.; Isailovic, D.; McMillan, R. A.; Conticello, V. P. *Biopolymers* **2003**, *70*, 158−168.
(20) Wishart, D. S.; Sykes, B. D.; Richards, F. M. *J. Mol. Biol.* **1991**, *222*, 311−333.
(21) Iwadate, M.; Asakura, T.; Williamson, M. P. *J. Biomol. NMR* **1999**, *13*, 199−211.
(22) Wang, Y.; Jardetzky, O. *Protein Sci.* **2002**, *11*, 852−861.
(23) Hong, M.; Jakes, K. *J. Biomol. NMR* **1999**, *14*, 71−74.
(24) Reiersen, H.; Clarke, A. R.; Rees, A. R. *J. Mol. Biol.* **1998**, *283*, 255−264.
(25) Schmidt-Rohr, K.; Hong, M. *J. Am. Chem. Soc.* **2003**, *125*, 5648−5649.
(26) Rhim, W.-K.; Elleman, D. D.; Vaughan, R. W. *J. Chem. Phys.* **1973**, *58*, 1772−1773.

tion, thus reducing the undesired REDOR dephasing due to natural abundance aliphatic carbons and improving the accuracy of the H^N-CO distance measurement. During this rotor period, a WIM sequence[27] was applied on the ^1H channel to suspend ^1H chemical shift and dipolar evolution. After the C−H REDOR period, a short Lee-Goldberg (LG) CP of 100 μs selectively transferred the ^1H magnetization to ^{15}N. In this way, the REDOR dephasing of only the amide proton was detected. Two experiments were conducted for each REDOR mixing time, one without the ^{13}C π pulses (S_0) and the other with the ^{13}C pulses (S). The time-dependent ratio S/S_0 signified the coupling strength. The sample was spun at a slow speed of 3.742 kHz to optimize MREV-8 performance.

To selectively detect the signals of molecules with short C−H and C−N distances, we converted the ^{15}N-detected C−H REDOR experiment to ^{13}C detection by appending a $^{15}N-^{13}C$ polarization transfer step after $^1H-^{15}N$ CP. The signals of molecules with a long C−N distance were largely suppressed due to inefficient $^{15}N-^{13}C$ transfer. The polarization transfer was achieved using a TEDOR pulse train (Figure 1b) for 2m rotor periods.[28] The TEDOR sequence was found to be far more efficient than $^{15}N-^{13}C$ CP for transferring the polarization. To enhance the sensitivity of this TEDOR-filterted REDOR experiment, we detected the ^{13}C spectrum using a Carr−Purcell echo train where one π pulse was applied every other rotor period.[29] This enhanced the sensitivity by about a factor of 5 compared to normal detection.

The V6 ^{13}CO to V9 ^{15}N distance was measured using a $^{13}C-^{15}N$ REDOR experiment.[30] A single 180° pulse was applied on the ^{13}C channel, while other 180° pulses were applied on ^{15}N and phase-cycled using the XY-16 scheme.[31] Since the ratio of labeled versus unlabeled ^{13}C sites is 100:14, natural abundance ^{13}CO contributed a constant intensity that was 12% of the reference signal (S_0) in both the S and S_0 spectra. Thus, the true REDOR dephasing was $(S/S_0)^{true} = (S^{obs} - c)/(S_0^{obs} - c)$, where $c = S_0^{obs} \times 12\%$. The sample was spun at 4 kHz for the C−N REDOR experiments.

For both the C−N and C−H REDOR spectra, S/S_0 values were evaluated by integrating the intensities of the carbonyl sideband manifold. REDOR curves were simulated using a Fortran program. For the C−H REDOR curves, the ideal MREV-8 scaling factor of 0.47 was used in calculating the dipolar couplings.

The distance distribution was assumed to consist of Gaussian functions $\sum_{i=1}^{2} \exp(-(r - r_{0,i})^2/2\sigma_i^2)$, where σ is the width and r_0 is the center of each Gaussian. The weights of the Gaussian peaks in the distribution function were calculated on the basis of the integrated peak areas. The composite REDOR curve was the weighted average of the individual single-distance REDOR curves.

Torsion Angle Measurements. ψ torsion angles were measured using the NCCN technique, which correlated the $^{15}N_i-^{13}C\alpha_i$ and $^{13}CO_i-^{15}N_{i+1}$ dipolar couplings to obtain the relative orientation of the two bonds.[32,33] $^{13}C\alpha-^{13}CO$ double quantum coherence, excited using the CMR7 sequence,[34] evolved under the $^{13}C-^{15}N$ dipolar coupling that was recoupled by a REDOR pulse train.[30] For each REDOR mixing time, a reference spectrum (S_0) without the ^{15}N 180° pulses and a dephased spectrum (S) with the ^{15}N pulses were measured. The average of the S/S_0 values of the Cα and CO signals was plotted as a function of the mixing time to yield a ψ-angle dependent curve. This was compared with simulated curves to obtain the best-fit ψ-angle. For the P7G8 peptide, only the ^{13}CO signal was analyzed since the Cα site was coupled to side-chain carbons as well.

The ϕ torsion angles of V6 and V9 were measured using the HNCH technique, which correlates the $^1H^N-^{15}N$ and $^{13}C\alpha-^1H\alpha$ dipolar couplings.[35] The conventional ϕ-angle was related to the NMR-based $H^N-N-C\alpha-H\alpha$ angle (ϕ_H) by $\phi = \phi_H + 60°$. We used the pulse sequence version with doubling of the H−N dipolar coupling to increase the angular resolution of the experiment.[36] The samples were spun at 5−6 kHz for the NCCN experiments and at 3.472 kHz for the HNCH experiment to optimize ^1H homonuclear decoupling by MREV-8.[26]

Chemical Shift Anisotropy (CSA) Determination. The ^{13}C CSA patterns of unlabeled poly(Lys-25) and $(VPGVG)_3$ were measured using the two-dimensional (2D) SUPER technique.[37] The experiment recoupled the CSA interaction by 2π pulses placed at calculated time points in a rotor period.[38] The rf field strength of the 2π pulses was 12.12 times of the spinning speed. A ^1H decoupling field of ~83 kHz was used during the ^{13}C 2π pulses. For the $^{13}C\alpha-^{13}CO$ doubly labeled G8V9 sample, a modified SUPER experiment incorporating a ^{13}C DANTE pulse train was used to remove the Cα−CO homonuclear dipolar interaction.[39] Slow spinning speeds of 2.5−3.0 kHz were used in these experiments. The V6 ^{13}CO CSA was measured by a static CP experiment on the singly ^{13}C-labeled V6V9 sample. In this article, we describe the anisotropic chemical shifts by the span Ω, defined as $\Omega = \delta_{11} - \delta_{33}$, and the asymmetry parameter η, defined as $(\delta_{22} - \delta_{11})/(\delta_{33} - \delta_{iso})$ when δ_{11} is closer to the isotropic shift than δ_{33}, and $(\delta_{22} - \delta_{33})/(\delta_{11} - \delta_{iso})$ when δ_{33} is closer to the isotropic shift. The three principal values are designated according to the convention $\delta_{11} \geq \delta_{22} \geq \delta_{33}$. All ^{13}C chemical shifts are referenced to the β-glycine carbonyl peak (176.4 ppm). The ^{15}N chemical shifts are referenced to liquid ammonia indirectly through the ^{15}N chemical shift of *N*-acetyl-valine (122 ppm).

All structural modeling was carried out using the Insight II Biopolymer program (Accelerys, San Diego).

Results and Discussion

$(VPGVG)_3$ Peptide as a Model System for Elastin. Previous studies established that VPGVG peptides with five repeat units or less exhibit an inverse temperature transition similar to tropoelastin, the soluble precursor of elastin.[24] We chose $(VPGVG)_3$ as a model system for elastin, since it is the shortest peptide in which a central repeat unit is flanked by two neighboring pentameric units so that structural measurements can be made on the central unit without potential chain-end disorder. To verify the conformational similarity between $(VPGVG)_3$ and elastin, we compared the NMR chemical shifts of $(VPGVG)_3$ with those of the 81 kDa poly(Lys-25). The latter's similarity to elastin has been demonstrated based on temperature-dependent reversible coacervation and the morphology of cross-linked hydrogels.[40]

It is well-known that backbone ^{13}C and ^{15}N chemical shifts, both isotropic and anisotropic, depend sensitively on protein secondary structure.[20,41−44] These chemical shifts can be readily

(27) Caravatti, P.; Braunschweiler, L.; Ernst, R. R. *Chem. Phys. Lett.* **1983**, *100*, 305−310.
(28) Sinha, N.; Hong, M. *Chem. Phys. Lett.* **2003**, *380*, 742−748.
(29) Petkova, A. T.; Tycko, R. *J. Magn. Reson.* **2002**, *155*, 293−299.
(30) Gullion, T.; Schaefer, J. *J. Magn. Reson.* **1989**, *81*, 196−200.
(31) Gullion, T.; Baker, D. B.; Conradi, M. S. *J. Magn. Reson. (1969−1992)* **1990**, *89*, 479−484.
(32) Costa, P. R.; Gross, J. D.; Hong, M.; Griffin, R. G. *Chem. Phys. Lett.* **1997**, *280*, 95−103.
(33) Feng, X.; Eden, M.; Brinkmann, A.; Luthman, H.; Eriksson, L.; Graslund, A.; Antzutkin, O. N.; Levitt, M. H. *J. Am. Chem. Soc.* **1997**, *119*, 12006−12007.
(34) Rienstra, C. M.; Hatcher, M. E.; Mueller, L. J.; Sun, B. Q.; Fesik, S. W.; Griffin, R. G. *J. Am. Chem. Soc.* **1998**, *120*, 10602−10612.
(35) Hong, M.; Gross, J. D.; Griffin, R. G. *J. Phys. Chem. B* **1997**, *101*, 5869−5874.
(36) Hong, M.; Gross, J. D.; Rienstra, C. M.; Griffin, R. G.; Kumashiro, K. K.; Schmidt-Rohr, K. *J. Magn. Reson.* **1997**, *129*, 85−92.
(37) Liu, S. F.; Mao, J. D.; Schmidt-Rohr, K. *J. Magn. Reson.* **2002**, *155*, 15−28.
(38) Tycko, R.; Dabbagh, G.; Mirau, P. *J. Magn. Reson.* **1989**, *85*, 265−274.
(39) Hong, M.; Yao, X. *J. Magn. Reson.* **2003**, *160*, 114−119.
(40) McMillan, R. A.; Conticello, V. P. *Macromolecules* **2000**, *33*, 4809−4821.
(41) Havlin, R. H.; Le, H.; Laws, D. D.; de Dios, A. C.; Oldfield, E. *J. Am. Chem. Soc.* **1997**, *119*, 11951−11958.
(42) Tjandra, N.; Bax, A. *J. Am. Chem. Soc.* **1997**, *119*, 9576−9577.
(43) Yao, X.; Hong, M. *J. Am. Chem. Soc.* **2002**, *124*, 2730−2738.
(44) Yao, X.; Yamaguchi, S.; Hong, M. *J. Biomol. NMR* **2002**, *24*, 51−62.

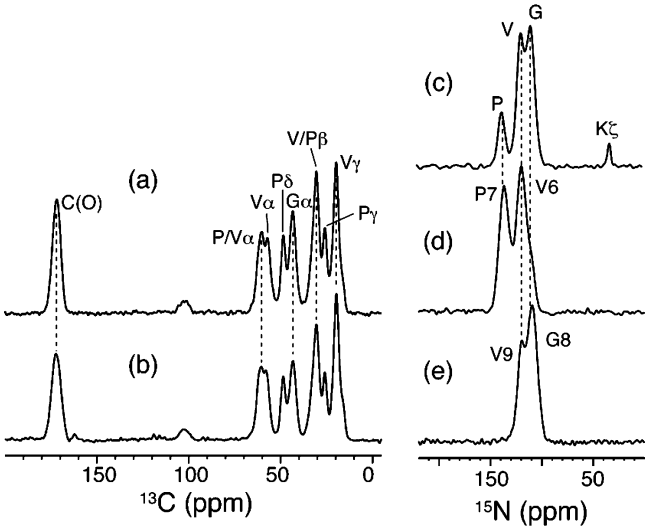

Figure 2. ^{13}C and ^{15}N MAS spectra of poly(Lys-25) and $(VPGVG)_3$. (a) Poly(Lys-25) ^{13}C spectrum. (b) $(VPGVG)_3$ ^{13}C spectrum. (c) Poly(Lys-25) ^{15}N spectrum. (d) ^{15}N spectrum of V6P7. (e) ^{15}N spectrum of G8V9. The chemical shifts of the small peptide are identical with the chemical shifts of the protein.

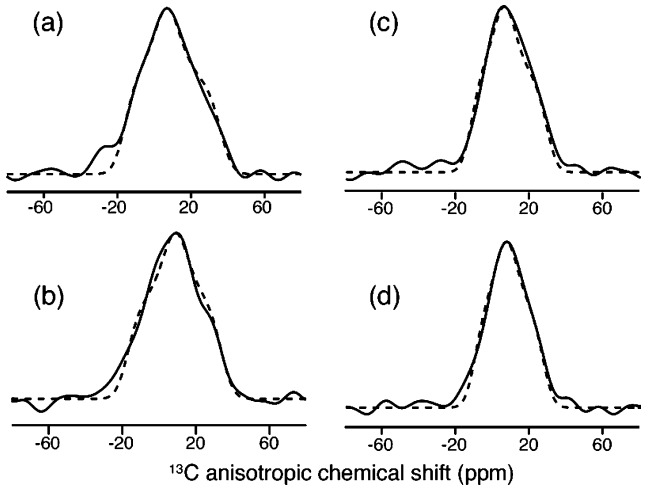

Figure 3. Cα CSA powder patterns of unlabeled poly(Lys-25) and $(VPGVG)_3$ extracted from 2D SUPER spectra. Solid line: experimental spectra. Dashed line: best fit. (a) Poly(Lys-25) Gly Cα. Best fit: $\Omega = 52$ ppm, $\eta = 0.85$. (b) $(VPGVG)_3$ Gly Cα. Best fit: $\Omega = 51$ ppm, $\eta = 0.97$. (c) Poly(Lys-25) Pro/Val-1 Cα. Best fit: $\Omega = 41$ ppm, $\eta = 0.84$. (d) $(VPGVG)_3$ Pro/Val-1 Cα. Best fit: $\Omega = 37$ ppm, $\eta = 0.89$.

extracted from 1D MAS spectra and 2D SUPER spectra. The ^{13}C CP spectra of poly(Lys-25) and $(VPGVG)_3$ are shown in Figure 2a,b. They exhibit almost identical isotropic shifts and line widths, indicating qualitatively that the two samples have the same conformation. To complement the isotropic shifts, we measured the ^{13}C anisotropic chemical shifts in unlabeled poly(Lys-25) and $(VPGVG)_3$ using the SUPER technique.[37] Overall, the span Ω and the asymmetry parameter η are similar between the two samples. The powder patterns of Gly Cα and Pro/Val-1 Cα are shown in Figure 3 along with their best fits. For Gly Cα, Ω and η are 52 ppm and 0.85 in poly(Lys-25) and 51 ppm and 0.97 in $(VPGVG)_3$. For Pro/Val-1 Cα, Ω and η are 41 ppm and 0.84 in poly(Lys-25) and 37 ppm and 0.89 in $(VPGVG)_3$. Further verification of the structural similarity of $(VPGVG)_3$ and poly(Lys-25) was obtained from ^{15}N isotropic chemical shifts.[20,45] Figure 2c−e shows 1D ^{15}N spectra of ^{15}N uniformly labeled poly(Lys-25), and ^{15}N doubly labeled V6P7 and G8V9. It can be seen that the isotropic shifts of Val, Gly, and Pro in $(VPGVG)_3$ match those in poly(Lys-25) well.

Since the carbon CSA spectra from the unlabeled peptide and protein samples have unavoidable resonance overlaps, we compared the single-site CSA of ^{13}C-labeled samples whenever available. The Cα CSA of the Gly residue following Pro in poly(Lys-25) has been previously measured using a selective polarization transfer method combined with the SUPER experiment.[46] The span is 50 ppm and η is 0.93. In $(VPGVG)_3$, the corresponding G8 Cα CSA is now determined on the G8V9 sample using homonuclear decoupled SUPER[39] (see Figure 10). A span of 50 ppm and an η of 0.92 are found. Thus, both isotropic and anisotropic chemical shifts indicate that $(VPGVG)_3$ has nearly identical conformation as poly(Lys-25), and thus is a suitable model system for elastin.

V6 ^{13}CO−V9 ^{1}H^{N} Distance. The central hypothesis of the β-spiral model for elastin is that the Pro-Gly linkage forms a type II β-turn.[9,10] However, this turn structure has not been directly determined in the solid state on a linear peptide. To test the existence of a tight turn structure at the Pro-Gly pair, we measured the V6 CO−V9 H^{N} distance (Figure 4a) using our recently developed C−H REDOR technique.[25] The C−H REDOR dephasing data, S/S_0, is shown in Figure 4b. The main feature of the data is that it cannot be fit to a single distance. The initial decay within the first ∼2 ms agrees well with a 4.0 Å distance, but above 3 ms the experimental S/S_0 steers significantly above the 4.0 Å curve. This flattening of the S/S_0 curve does not result from pulse imperfections, as C−H distances up to 6.0 Å at mixing times up to 10 ms have been measured in an intermolecular mixture of ^{13}CO and ^{15}N-labeled *N*-*t*-BOC-glycine sample. There, low S/S_0 values of less than 0.2 were found.[25] Therefore, the fast initial decay and the flattening of the C−H REDOR data at long mixing times suggest the coexistence of intramolecular spin pairs with short and long distances, reflecting both compact and extended structures of the peptide.

Using a simple bimodal distribution with suitable Gaussian widths (vide infra), we obtained excellent fit by combining a short C−H distance of 3.3 ± 0.2 Å with a weight of 35% and a long distance of 7.0 ± 0.5 Å with a weight of 65% (Figure 4c). The fractions of the short and long distances, 35 and 65%, were determined from the height of the S/S_0 plateau. Since the short distance that gives rise to the initial decay has nearly zero intensity at long times, the S/S_0 values at long mixing times mainly result from the weak coupling. Thus, the weights of the two components were determined independently of the coupling strengths, which were obtained from the oscillation frequencies of the REDOR curve. The strong coupling or short distance is constrained tightly by the fast initial decay (Figure 4b). On the other hand, the long distance component has a physical upper limit of 7.8 Å, obtained when Pro and Gly adopt the most extended conformation: Pro (−70°, 180°) and Gly (180°, 180°). Under this condition, both C−H and C−N distances reach a maximum value of 7.8 Å. Thus, the distance distribution shown in Figure 4c has a cutoff at 7.8 Å. The use of a broader Gaussian width of 1.0 Å for the long distance component to reflect more

(45) Zhang, H.; Neal, S.; Wishart, D. S. *J. Biomol. NMR* **2003**, *25*, 173−195.
(46) Hong, M.; McMillan, R. A.; Conticello, V. P. *J. Biomol. NMR* **2002**, *22*, 175−179.

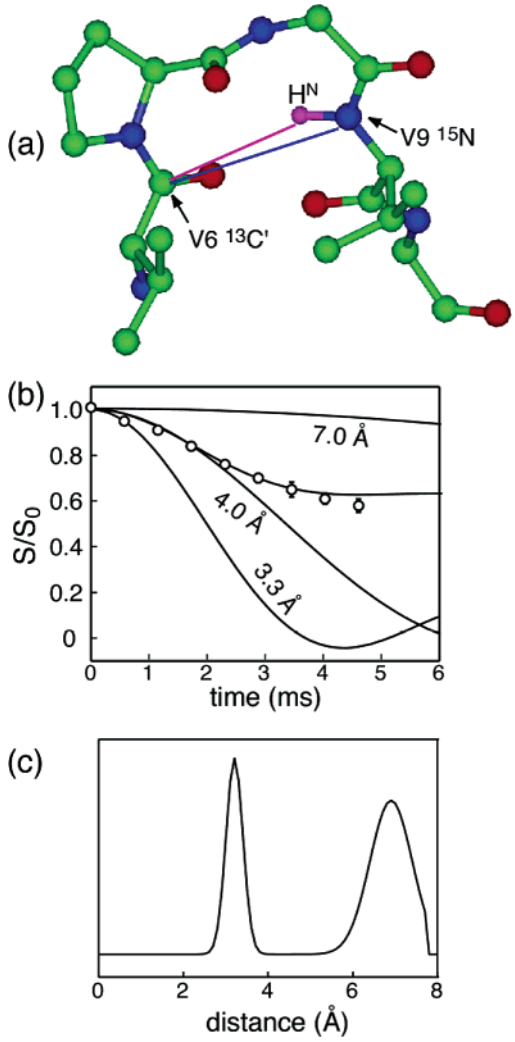

Figure 4. V6 ^{13}CO−V9 ^{1}H^{N} distance. (a) Schematic structure of $(VPGVG)_3$ illustrating the C−H and C−N distances of interest. (b) S/S_0 as a function of mixing times. Error bars are mostly smaller than the symbol size. Best fit: 3.3 ± 0.2 Å at 35% and 7.0 ± 0.5 Å at 65%. No single distance curves fit the data. The best attempt of 4.0 Å deviates from the experimental data at long times. (c) Best-fit two-distance distribution.

disorder, while producing a reasonable fit to the C−H REDOR curve, does not agree with other data, as we show below in Figure 11.

V6 ^{13}CO−V9 ^{15}N Distance. The same ^{13}C,^{15}N-labeled V6V9 sample was also used to measure the V6 CO−V9 N distance. Figure 5a shows the C−N S/S_0 values after correcting for natural abundance ^{13}C contributions. Similar to the C−H data, the C−N REDOR curve cannot be fit to a single distance. A distance of 5.0 Å fits the initial decay up to 20 ms, but then deviates significantly from the data at longer mixing times. Best fit to the experimental data was obtained using a double-Gaussian distribution with 35% of a short distance 4.3 ± 0.2 Å and 65% of a longer distance 7.2 ± 0.5 Å (Figure 5b). This combination satisfies the constraint that in each conformation, the C−N distance cannot differ by more than 1.0 Å from the C−H distance, since the N−H bond that forms a triangle with the C−H and C−N vectors is ∼1.0 Å long. Since the C−H distances are found to be 3.3 and 7.0 Å, the C−N distance must fall in the range of 2.3−4.3 Å in the compact structure and 6−7.8 Å in the extended structure. Again, the initial slope of the experimental C−N REDOR data constrains the short

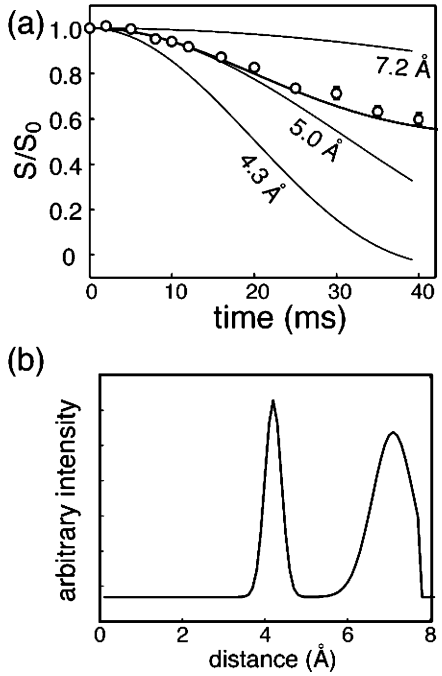

Figure 5. V6 ^{13}CO−V9 ^{15}N distance. (a) S/S_0 data as a function of mixing times. Best fit: 4.3 ± 0.2 Å at 35% and 7.2 ± 0.5 Å at 65%. No single distance fits the data. The best attempt of 5.0 Å deviates from the data at long times. (b) Best-fit distance distribution.

distance well. For the weak coupling component, simulations show that a distance significantly below 7.0 Å does not fit the data (see Figure 11a), because it makes the REDOR curve drop noticeably below the experimental data.

In both the C−H and C−N distance measurements, the shorter distance has a narrower distribution than the longer one. This is reasonable since the compact structure should form a hydrogen bond in each repeat unit, thus restricting the conformational space of the molecule, while the extended structure lacks a hydrogen bond, thus sampling a larger conformational space.

Since long mixing times of up to 40 ms were used in the C−N REDOR experiment, it is important to verify that the plateau of the REDOR curve that signifies long distances does not result from accumulated pulse imperfections.[47] To test this, we measured the intermolecular C−N distance in the 1:1 mixture of ^{13}CO and ^{15}N-labeled *N*-*t*-BOC-glycine. The longest distance present in this mixture with more than 25% probability is 6.08 Å, while the shortest distance (with 37.5% probability) is 3.65 Å. The experimental C−N REDOR data (not shown) agree well with the calculated REDOR curves based on the crystal structure. The minimum S/S_0 is 0.3 at a mixing time of 30 ms. Thus, the large S/S_0 values (0.6−0.7) of V6V9 at similar mixing times do not result from experimental imperfections. Further, by choosing ^{13}C detection for the C−N REDOR measurement, we minimize the number of natural-abundance dephasing spins, since ^{15}N natural abundance is low (0.34%) and nitrogen atoms occur less often than carbon in proteins.

C−N-Filtered V6 ^{13}CO−V9 ^{1}H^{N} Distance. To unambiguously prove the existence of a compact structure in VPGVG, we carried out a C−H REDOR experiment with an additional C−N dipolar filter. Instead of ^{15}N detection of the V6V9 C(O)−

(47) (a) Chan, J. C.; Eckert, H. *J. Magn. Reson.* **2000**, *147*, 170−178. (b) Sinha, N.; Schmidt-Rohr, K.; Hong, M. *J. Magn. Reson.* **2004**, in press.

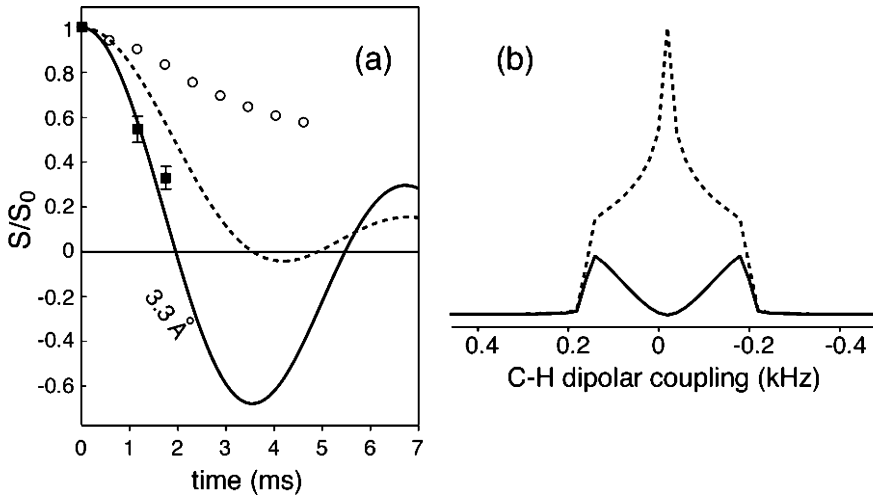

Figure 6. V6 ^{13}CO−V9 ^{1}H^{N} distance measured with a ^{13}C−^{15}N TEDOR filter of 18 ms. (a) S/S_0 (■). The unfiltered C−H REDOR decay (○) is reproduced for comparison. The simulated C−H REDOR curves for 3.3 Å with the C−N TEDOR filter (solid line) and without the C−N filter (dashed line) both decay much faster than the unfiltered C−H data. The C−N filtered 3.3 Å C−H REDOR curve fits the data quantitatively. (b) Simulated REDOR spectra for a 3.3 Å C−H distance without the C−N filter (dashed line) and with the C−N filter (solid line). TEDOR increases the relative intensity of the 0° edge while decreasing the intensity of the isotropic peak.

H^{N} dipolar coupling, we can transfer the V9 ^{15}N magnetization back to V6 ^{13}CO using a TEDOR sequence[48] and detect the ^{13}C signal (Figure 1b). If the peptide indeed adopts two types of conformations around PG residues, then the C−N dipolar coupling for the long V6V9 distance (7.2 Å) is so much weaker than that for the short distance (4.3 Å) that a short C−N TEDOR mixing time should selectively detect only those molecules with the short C−N distance. Since these molecules also have a short C−H distance, the C−H REDOR curve should decay much faster than the unfiltered data in Figure 4.

Figure 6a shows the C−N-filtered C−H REDOR data (squares) for C−H mixing times of 1.15 and 1.73 ms. A TEDOR mixing time of 18 ms was used. The two S/S_0 values drop dramatically below the unfiltered C−H REDOR data, thus proving unequivocally that a fraction of the peptide indeed adopts a compact structure with short V6−V9 distances. Interestingly, the simulated 3.3 Å C−H REDOR curve without the C−N filter (dashed line) is higher than the experimental S/S_0 decays. This can be understood from the fact that the C−N TEDOR filter imposes an orientational factor of $\sin^2(\omega_{CN}\tau_{CN})$ to the REDOR time signal and changes powder averaging. Since the C−H and C−N vectors are roughly collinear, this orientational factor preferentially selects the signals of the C−H vectors that are parallel to the magnetic field, which have stronger dipolar couplings. Figure 6b shows the unfiltered C−H REDOR line shape for a 3.3 Å distance (dashed line) and the TEDOR-filtered REDOR line shape (solid line). The TEDOR transfer step changes the normal $\eta = 1$ REDOR line shape to one with the strongest intensities at the 0° edge and vanishing intensities at the magic angle orientation. The Fourier transform of this TEDOR-filtered REDOR spectrum gives the solid line in Figure 6b. The agreement with the experiment is excellent.

Distance Distribution in Diluted Peptide. The isotopically labeled V6V9 peptide used for the above two distance measurements was lyophilized as well as undiluted. The former prompts the question whether the observed structure distribution is an intrinsic property of the amino acid sequence or a result of lyophilization. The lack of dilution raises the question whether intermolecular couplings could give rise to the slow REDOR decays seen at long mixing times. Such a three-spin scenario in which a strong intramolecular coupling combines with a weak intermolecular coupling to give a distributed REDOR curve can in principle be ruled out, because any weak couplings would have been truncated by the strong couplings, preempting the observation of the S/S_0 plateau at long mixing times. In other words, the coexistence of a fast initial decay and a very slow long time decay must result from two independent spin pairs with different distances. These can only be intramolecular in origin.

To verify experimentally that the observed distance heterogeneity is a consequence of neither lyophilization nor intermolecular effects, we diluted the labeled V6V9 peptide with 80% unlabeled peptide, dried the mixture from an aqueous solution over a period of one week, and measured the C−H and C−N REDOR curves. The ^{13}C and ^{15}N line widths are barely affected by the slow drying process, indicating that conformational heterogeneity remains. The C−H and C−N REDOR data for this 20% diluted and slow-dried sample are shown in Figure 7. The C−N REDOR experiment used composite pulses on the ^{15}N channel and EXORCYCLE on the ^{13}C channel to compensate for pulse imperfections.[47] It can be seen that the experimental data remain incompatible with single-distance REDOR curves, indicating unambiguously that intermolecular couplings do not cause the distance distribution in the undiluted sample. The equilibrium S/S_0 values for both the C−H and C−N REDOR are slightly reduced compared to the lyophilized sample, indicating that the percentages of the short and long distances are modified by the slow drying process. Best-fit simulation yields two C−N distances of 4.0 ± 0.2 and 7.0 ± 0.5 Å at a ratio of 45:55%, while the C−H data is best-fit with a combination of 3.3 ± 0.2 and 6.7 ± 0.5 Å at the same ratio. These distances agree with the results of the lyophilized and undiluted peptide within experimental uncertainty. Thus, the slow drying process mainly increased the fraction of the compact structure by 10%. Conformational distribution remains, indicating that this is an inherent feature

(48) Hing, A. W.; Vega, S.; Schaefer, J. *J. Magn. Reson.* **1992**, *96*, 205−209.

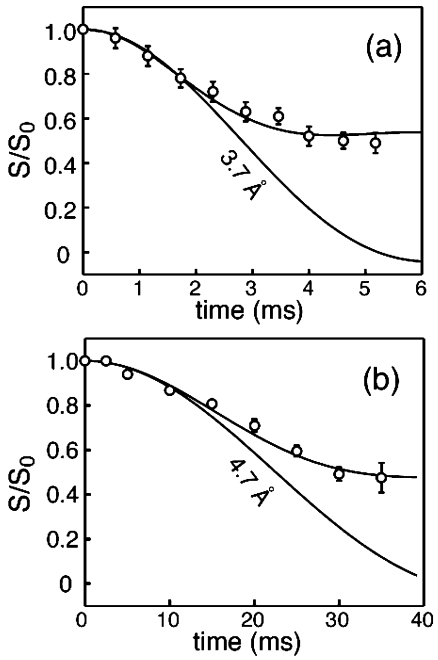

Figure 7. REDOR distances of 20% diluted V6V9 peptide slowly dried from aqueous solution. (a) V6 CO−V9 H^N distance. Best fit: 45% of 3.3 ± 0.2 Å and 55% of 6.7 ± 0.5 Å. The simulated curve for a single C−H distance of 3.7 Å fits the initial decay but not the long time behavior. (b) V6 CO−V9 N distance. Best fit: 45% of 4.0 ± 0.2 Å and 55% of 7.0 ± 0.5 Å. The simulated curve for a single C−N distance of 4.7 Å fits the initial decay but not the long time data.

of the VPGVG sequence. Since the torsion angle and CSA measurements were conducted on lyophilized samples, for consistency we consider only the structure distribution of the lyophilized peptide in the remainder of the article.

***ψ, ϕ* Torsion Angles.** The V6−V9 C−H and C−N distances restrain the P7 and G8 torsion angles. To complement the distance constraints, we directly measured the ψ and ϕ torsion angles in $(VPGVG)_3$ using the NCCN and HNCH techniques. The REDOR experiments are sensitive to short distances or strong couplings but do not have high precision for the long distances. In contrast, the NCCN and HNCH experiments are more sensitive to large torsion angle values that give long distances, and thus they detect the presence of extended structures well. The P7 ϕ-angle is fixed by the pyrrolidine ring geometry to be −70°; thus the only free variables in the PG pair are P7 ψ and G8 ϕ and ψ. Beyond the PG unit, the torsion angles of V6, V9, and G10 were also measured.

The ψ-angle dependent NCCN curves of G8, P7, and V6 are shown in Figure 8. Since the NCCN and HNCH techniques have an inherent double degeneracy and cannot distinguish the sign of the angles, we report only the absolute value of the measured ψ- and ϕ_H-angles. The G8 (Figure 8a) and P7 (Figure 8b) data, except for the time points above 1.5 ms, can be reasonably fit with a torsion angle of $\psi = 150°$ (dotted lines), suggesting that a majority of the molecules adopts an extended structure at the PG residues. To test if the deviation above 1.5 ms is due to experimental artifacts, we performed the NCCN experiment on a polycrystalline sample (U−^{13}C,^{15}N) Gly-(^{15}N) Ala-Leu, where the Gly ψ-angle is −150°.[49] The experimental NCCN data (Figure 8d) show excellent agreement with the simulated curve at long mixing times. Thus, the difference between the experiment and the single-angle simulation for G8 and P7 has a real structural origin. Since the REDOR measurements indicate the presence of a compact structure in addition to extended structures, we used two-angle simulations with the same weighting factors of 35:65% as the distance finding. For G8, a combination of $\psi = 20 \pm 20°$ at 35% and $\psi = 158 \pm 5°$ at 65% (Figure 8a, solid line) improves the fit at long mixing times. The P7 data is better fit by a ψ-angle combination of $120 \pm 20°$ at 35% and $160 \pm 5°$ at 65% (Figure 8b). The small error bar for the large ψ-angle component is due to the maximum angular resolution of the NCCN technique at $\psi = 180°$.

For V6 (Figure 8c), V9, and G10, best-fit ψ-angles of 145°, 145°, and 150°, respectively, were obtained. These torsion angles refer to the dominant conformation, since the lack of distance constraints for these residues precludes the extraction of torsion angle distributions. However, given the clear evidence of structure distribution for P7 and G8, conformational distribution may be present for these residues as well.

The ϕ-angles of V6 and V9 were measured by the HNCH experiment (Figure 9). The V6 data is best fit with a ϕ_H-angle of ±156°, which corresponds to a ϕ-angle of −96° or −144°. For V9, a ϕ_H-angle of ±152° is found, which is equivalent to a ϕ-angle of −92° or −148°. Within each pair of degenerate values, the more negative numbers, −144° and −148°, are more likely since they combine with the ψ-angles to indicate the antiparallel β-strand structure for these residues.

Gly 8 Cα CSA. The CSA spectrum of G8 Cα was measured using the homonuclear decoupled SUPER experiment (Figure 10, thick line). The experimental pattern is relatively broad due to the amorphous nature of the peptide. Thus, CSA simulation emphasized the width of the pattern and the frequency of the central principal value. Best-fit simulation yielded a span of 50 ± 6 ppm and an asymmetry parameter of 0.92.

To assess if the measured chemical shift tensor values agree with the conformations determined from the distance and torsion angle measurements, we compared the experimental CSA with the calculated CSA values (chemical shielding calculator: http://waugh.cchem. berkeley.edu/∼bob/cs.html) for various torsion angles. For example, for the extended structure shown in Figure 12c ($\phi = -93°$ and $\psi = +154°$), the predicted Gly chemical shielding principle values are $\sigma_{11} = 130$ ppm, $\sigma_{22} = 155$ ppm, and $\sigma_{33} = 180$ ppm. For the β-turn structure shown in Figure 12b ($\phi = +96°$ and $\psi = -7°$), the predicted principal values are $\sigma_{11} = 128$ ppm, $\sigma_{22} = 156$ ppm, and $\sigma_{33} = 178$ ppm. We converted the absolute shielding values σ to chemical shifts δ using $\delta = (\sigma_{ref} - \sigma)/(1 - \sigma_{ref})$.[50,51] Ignoring the isotropic term, we readily obtained the theoretical span Ω and asymmetry parameter η. In this way, we found that the extended conformation has $\Omega = 50$ ppm and $\eta = 1.0$, while the compact structure has $\Omega = 50$ ppm and $\eta = 0.82$. Both these CSA values are close to the experimental result. Thus, not surprisingly, the predicted powder pattern that combines 65% of the extended structure with 35% of the compact structure also agrees well with the experimental spectrum.

(49) Chaturvedi, S.; Go, K.; Parthasarathy, R. *Biopolymers* **1991**, *31*, 397−407.

(50) Jameson, C. J. *Solid State Nucl. Magn. Reson.* **1998**, *11*, 265−268.

(51) Havlin, R. H.; Laws, D. D.; Bitter, H. L.; Sanders, L. K.; Sun, H.; Grimely, J. S.; Wemmer, D. E.; Pines, A.; Oldfield, E. *J. Am. Chem. Soc.* **2001**, *123*, 10362−10369.

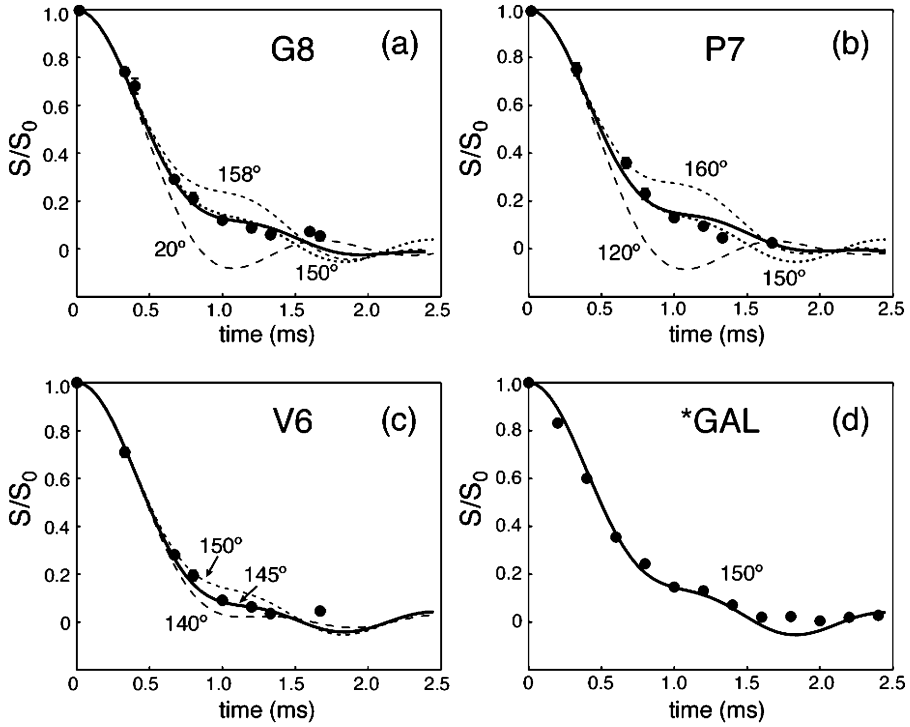

Figure 8. ψ torsion angles measured by the NCCN experiment. (a) G8. Dash and dotted lines are single-angle simulations. Solid line: the weighted average of 20° (35%) and 158° (65%). (b) P7. Dash and dotted lines are single-angle simulations. Solid line: the average of 120° (35%) and 160° (65%). (c) V6. Best fit: $\psi = 145°$. (d) Gly in GAL. Best fit: $\psi = 150°$. Error bars are mostly smaller than the symbol size.

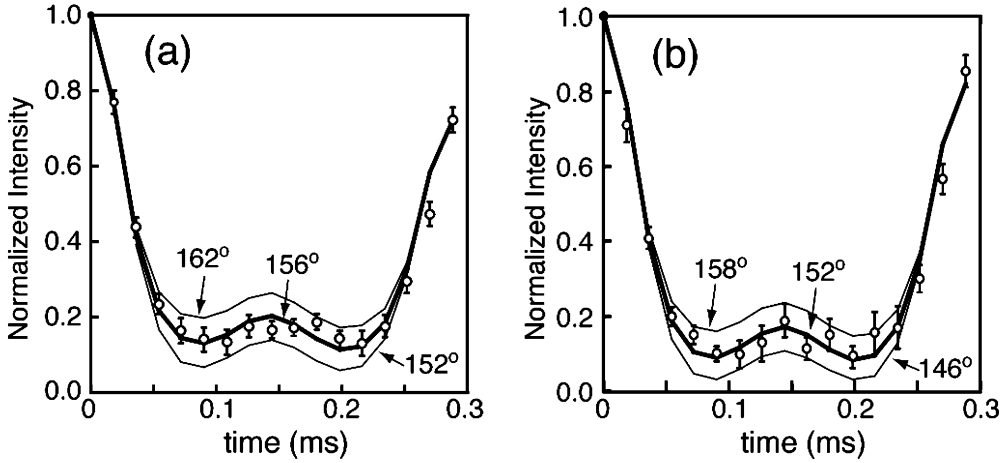

Figure 9. ϕ torsion angles measured by the HNCH experiment. (a) V6. Best fit: $\phi_H = \pm 156 \pm 6°$, corresponding to $\phi = -96 \pm 6°$ or $-144 \pm 6°$. (b) V9. Best fit: $\phi_H = \pm 152 \pm 6°$, corresponding to $\phi = -92 \pm 6°$ or $-148 \pm 6°$.

Interestingly, even a relatively small change of the Gly torsion angles from the extended conformation measured here to an ideal parallel β-strand structure of ($-120°$, $+120°$) makes a significant difference to the Gly CSA. This is shown in Figure 10b, where the calculated powder pattern for 35% of the β-turn and 65% of the ideal parallel β-strand is clearly narrower than the experimental spectrum. Similarly, the classical antiparallel β-sheet structure ($-135°$, $+135°$) can be ruled out. Therefore, the extended structure of the PG pair is not equivalent to the ideal β-strand structure.

Structure Distribution of $(VPGVG)_3$. On the basis of the distance and torsion angle results on $(VPGVG)_3$, we can now assess the suitability of the Gaussian width of 0.5 Å for the long C−H and C−N distances in the bimodal distributions (Figures 4c and 5b). The question is whether the peptide has a more disordered and heterogeneous structure that would be reflected as a significantly larger Gaussian width. Figure 11 shows several distance simulations using a Gaussian width of 1.0 Å for the long distance component while keeping both the center (4.3 Å for C−N and 3.3 Å for C−H) and width (0.2 Å) of the short distance the same. Figure 11a shows that with the broadened long distance distribution, the C−N REDOR data cannot be fit as long as the percentages of the two Gaussian peaks are kept as 35 and 65%. Simulated curves using a long distance component of 6.5−7.5 Å exhibit significantly more dephasing than the experimental data. In other words, the experimentally observed slow C−N REDOR decay at long times requires a high percentage of long distances above 7.0 Å, which is not satisfied when a broader distribution is used.

If we adjust the ratio of the two Gaussian peaks to 25:75%, then the C−N data can be well fit by two distances centered at 4.3 and 7.0 Å (Figure 11b). But the C−H REDOR data cannot

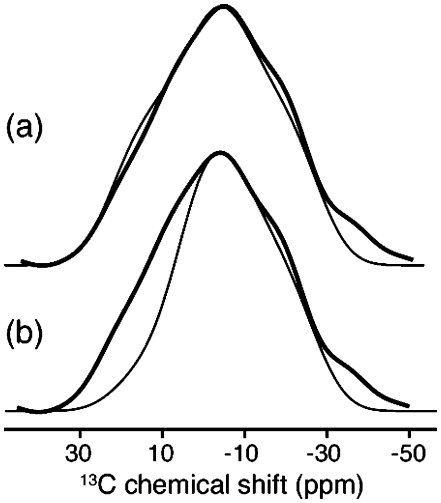

Figure 10. G8 Cα CSA powder pattern extracted from a 2D SUPER spectrum. The experiment spectrum (thick line) is superimposed with simulated spectra (thin line) based on calculated CSAs. (a) Simulated spectrum for 35% (+96°, −7°) and 65% (−93°, +154°). The torsion angles correspond to the structure in Figure 12b. (b) Simulated spectrum for 35% (+96°, −7°) and 65% (−120°, +120°). The latter is the ideal parallel β-strand structure. The simulated spectrum is much narrower than the experimental line shape, ruling out the ideal parallel β-sheet as a possible conformation.

be fit. The best simulation, which still deviates from the experimental data at long times, centers the two Gaussian peaks at 3.1 and 6 Å. The short distance is 1.2 Å shorter than the short C−N distance of 4.3 Å, thus violating the requirement that the C−H and C−N distances be within 1 Å of each other due to the N−H bond length.

When we used an intermediate ratio of 30:70% for the two Gaussian peaks, we obtained reasonable although not perfect fit for the C−N data using distances of 4.3 ± 0.2 and 7.0 ± 1.0 Å. The corresponding best fit for the C−H data yields distances of 3.3 ± 0.2 and 6.0 ± 1.0 Å (Figure 11c). In other words, at this ratio, the C−H and C−N distances differ by the maximum amount of 1.0 Å in both the compact and extended structures. This means that the C, H, and N atoms fall nearly on a line in both conformations. A search of Pro and Gly torsion angles (vide infra) indicates that this is only possible if the Gly ψ-angle has small values of 40 ± 20° in both conformations. Without a large ψ-angle in either conformation, the experimental NCCN data of G8 cannot be fit, as shown in Figure 11d. Taken together, a broader distribution with a width of 1.0 Å for the long distance component does not agree with all experimental data. Thus, the heterogeneity of the extended conformation is adequately described by a distance uncertainty of ±0.5 Å.

Structure Model for $(VPGVG)_3$. We searched for the combinations of P7 and G8 torsion angles that satisfy all the distances, torsion angles, and CSAs measured here. The Pψ, Gϕ, and Gψ angles were varied at 20° increments, while the Pϕ angle was held at −70°. For torsion angle combinations that satisfy the distance constraints, we then examined their Gly Cα CSAs. Anisotropies that differ from the experimental data by more than 6 ppm were excluded. The torsion angles for the short and long distances were then assessed for their consistency with the NCCN data, using the ratio of 35:65% for the compact and the extended structures.

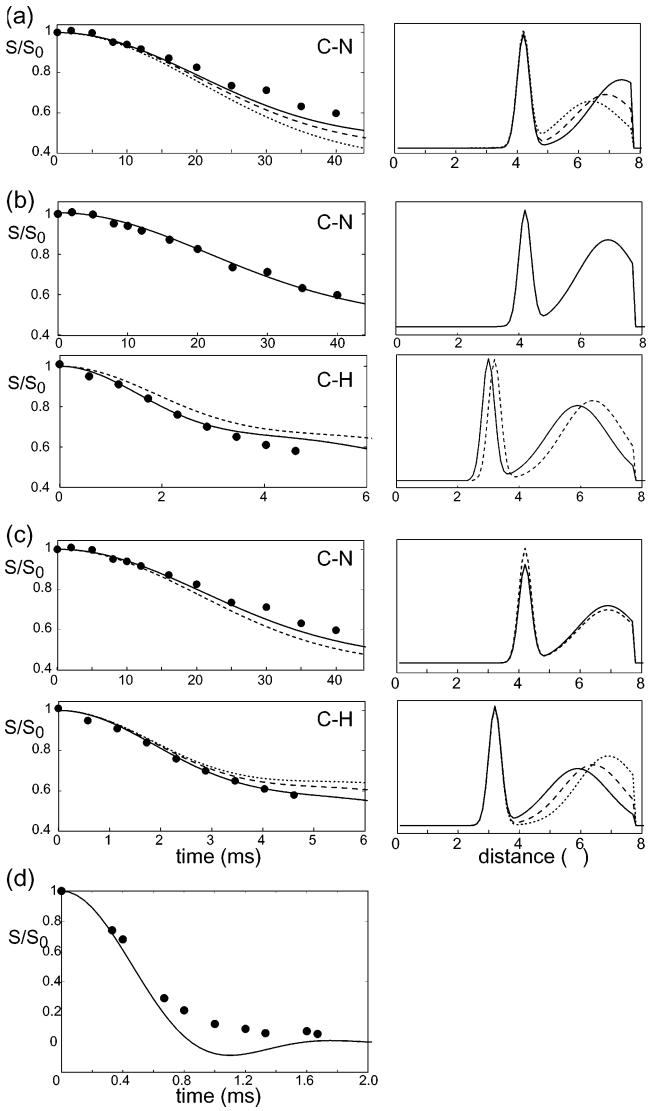

Figure 11. REDOR simulations using a broader Gaussian width of 1.0 Å for the long distance component. Right column shows the distribution functions corresponding to the distance fits. (a) C−N REDOR simulations with a ratio of 35:65% for the short and long distances. The short distance is fixed at 4.3 ± 0.2 Å. The long distances are 7.5 ± 1.0 Å (solid line), 7.0 ± 1.0 Å (dashed line), and 6.5 ± 1.0 Å (dotted line). All dephase more than the experimental data. (b) C−N and C−H REDOR simulations using a ratio of 25:75% for the short and long distances. For C−N, a combination of 4.3 ± 0.2 and 7.0 ± 1.0 Å fit the data well. For C−H, the (3.3 ± 0.2, 6.5 ± 1.0 Å) curve (dashed line) does not dephase enough. The best fit is (3.1 ± 0.2, 6.0 ± 1.0 Å) (solid line), but this violates the covalent geometry. (c) C−N and C−H REDOR simulations using a ratio of 30:70%. The C−N data is reasonably fit with 4.3 ± 0.2 and 7.0 ± 1.0 Å (solid line). For the C−H data, with the short distance at 3.3 ± 0.2 Å, long distances of 7.0 ± 1.0 Å (dotted line) or 6.5 ± 1.0 Å (dashed line) show too little dephasing, and 6.0 ± 1.0 Å (solid line) must be used. The combination of C−H and C−N distances of (3.3, 4.3 Å) for the compact structure and (6.0, 7.0 Å) for the extended structure is possible only if the Gly ψ-angle is 40 ± 20°. (d) Simulated NCCN curve for 40 ± 20° disagrees with the G8 experimental data.

Figure 12a summarizes the allowed Pro and Gly torsion angles in a Ramachandran diagram. The conformations that give rise to short V6V9 distances are labeled with a superscript *s*, while the conformations that yield long V6V9 distances are indicated with *l*. The extended structure is characterized by P7 ψ-angle of 160 ± 5° and G8 torsion angles of ($\phi = -90 \pm 20°$, $\psi = \pm 158 \pm 5°$). Since the negative ψ-angle conformation falls into a rarely populated region of the Ramachandran

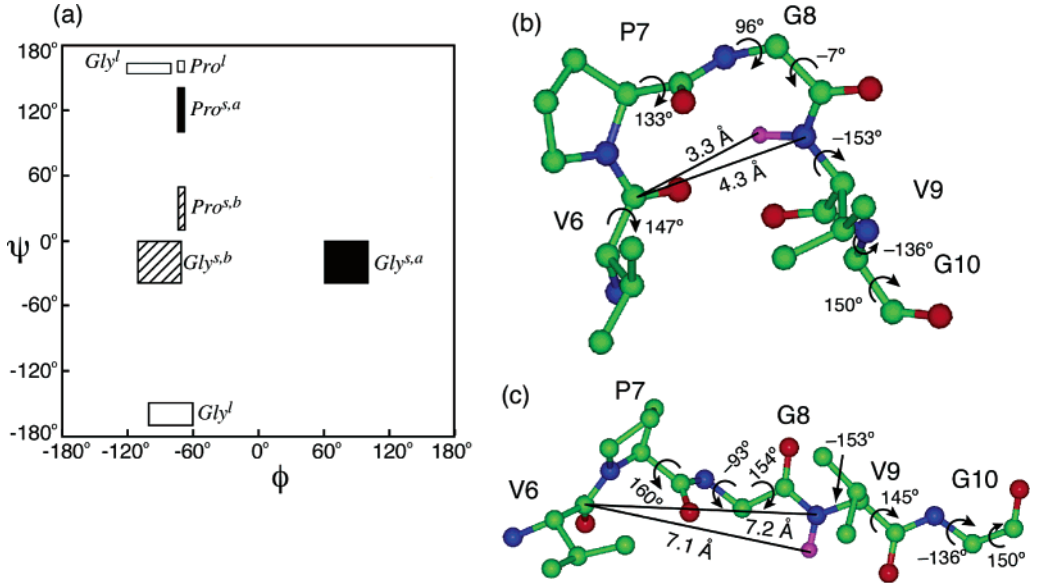

Figure 12. (a) P7 and G8 (ϕ, ψ) torsion angles restrained by the distances, torsion angles, and chemical shifts measured here. The compact structures with short V6V9 distances are labeled with a superscript *s*, while the extended structure with long V6V9 distances is labeled with *l*. (b) Model for one of the two compact structures (*s*, *a*) where P7 and G8 adopt type II β-turn torsion angles. (c) Model for the distorted β-strand conformation. The torsion angles in the two models are representative values within the allowed ranges shown in (a). For V6, V9, and G10, the torsion angles represent the dominant conformation and are the same in the two states.

Table 1. Torsion Angle Definitions, Predicted V6−V9 C−H and C−N Distances and G8 Cα Chemical Shifts for Different Types of β-Turns

β-turn type	P ϕ	P ψ	G ϕ	G ψ	C–N (Å)	C–H (Å)	Ω (ppm)
I	−70°	−30°	−90°	0°	3.8	2.7	49.1
II	−70°	120°	80°	0°	3.9	2.9	48.0
III	−70°	−30°	−60°	−30°	4.0	3.0	41.7
V	−70°	80°	80°	−80°	5.1	5.0	36.1
VIII	−70°	−30°	−120°	120°	5.7	5.4	32.8

diagram, the positive ψ-angle appears more likely for Gly. This PG conformation may be described as a distorted β-strand structure, since the ideal parallel and antiparallel β-strands have distinct ψ-angles of +120° and +135°, respectively.

Two compact structures were found to give the measured short V6V9 distances. One is the type II β-turn structure with P7 ($\phi = -70°$, $\psi = 120 \pm 20°$) and G8 ($\phi = 80 \pm 20°$, $\psi = -20 \pm 20°$). The other is characterized by Pro torsion angles ($\phi = -70°$, $\psi = 20 \pm 20°$) and Gly torsion angles ($\phi = -100 \pm 20°$, $\psi = -20 \pm 20°$). This structure does not correspond to any known β-turn.

The conformational search rules out all other known β-turns for the PG residues. Table 1 lists the torsion angle definitions, the predicted V6V9 C−H and C−N distances, and the predicted G8 Cα CSA for type I, type II, type III, type V, and type VIII β-turns. Only type II and type III β-turns yield distances consistent with the REDOR measurements; however, the type III turn would give much narrower G8 Cα CSA than the experimental spectrum. This leaves type II β-turn the only possible known β-turn that satisfies all constraints for the compact structure.

Figure 12b shows one of the two compact structures, the type II β-turn. While specific torsion angles were used to generate this model, they only represent a subset of the values within the allowed angular ranges shown in Figure 12a. The torsion angles and the short V6V9 distances in this structure predict a hydrogen bond between V6 O and V9 H^N, with a bond length

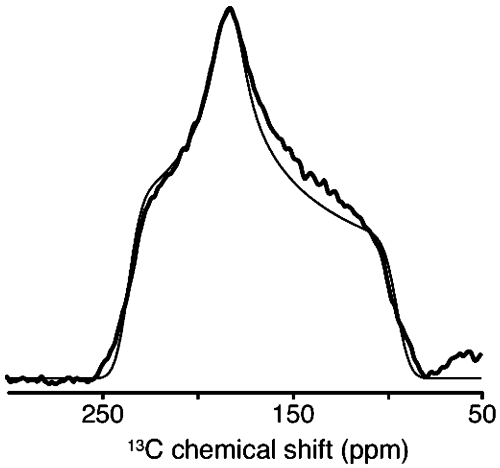

Figure 13. V6 ^{13}CO CSA powder pattern. The experimental spectrum (thick line) is best fit (thin line) using principle values of $\delta_{11} = 242.7$ ppm, $\delta_{22} = 184.7$ ppm, and $\delta_{33} = 87.7$ ppm.

R_{O-H} of 2.5 Å and a C═O−H^N angle of 124°, close to the optimum hydrogen bond angle of 120°.[52] Support for this hydrogen bond is provided by the V6 ^{13}CO chemical shift tensor. Both experiments and quantum chemical calculations have shown that hydrogen bonds deshield the δ_{22} principal value of the carbonyl chemical shift tensor, which points along the C═O bond, thus decreasing its asymmetry parameter.[52,53] Indeed, the V6 carbonyl CSA spectrum (Figure 13) exhibits a relatively small asymmetry parameter of 0.68, consistent with the presence of a hydrogen bond between V6 CO and V9 H^N. The second compact structure labeled as *s*,*b* has a R_{O-H} length of 2.3 Å, also consistent with hydrogen bonding.

The distorted β-strand structure is represented in Figure 12c. No intramolecular hydrogen bond is formed in this conformation. In both structures, the three other residues of the repeat

(52) de Dios, A. C.; Oldfield, E. *J. Am. Chem. Soc.* **1994**, *116*, 11485−11488.
(53) Gu, Z.; Zambrano, R.; McDermott, A. *J. Am. Chem. Soc.* **1994**, *116*, 6368−6372.

unit adopt (ϕ, ψ) angles that are consistent with the antiparallel β-strand conformation. Structure distribution is not directly measured for these residues but is likely to be present as well. The G10 ϕ-angle could not be measured by the HNCH experiment due to the presence of two Hα protons. But on the basis of the G10 Cα isotropic shift of 42.6 ppm, which is 0.7 ppm upfield from the random coil value,[45] we estimate its ϕ-angle to be about $-135°$.[21]

The presence of conformational distribution has been reported before in natural elastin as well as elastin-mimetic proteins. For example, infrared spectroscopy and circular dichroism experiments on human and bovine elastins found 35−45% of β-strand structure, 55−45% of turn or coil structures, and a low level of α-helix ($\sim$10%).[8,54] Molecular dynamics simulation of hydrated $(VPGVG)_{18}$ found $\sim$35% of type II β-turn conformation below the inverse temperature transition.[55] Tamburro and co-workers concluded that a mixture of folded and extended structures interchange within themselves.[1,15] Recently, Asakura and co-workers measured torsion angles of residues V1, V4, and G5 in $(VPGVG)_6$ by 2D exchange NMR under off-magic angle spinning.[56] They found that none of the spectra could be fit using a single conformation. A more detailed analysis on G5 indicated conformational distribution that is qualitatively consistent with our present study. Qualitative indication of elastin conformational heterogeneity was also observed from our previous ^{13}C line width analysis of poly(Lys-25).[17,19] The Cα intrinsic line widths were measured as $\sim$95 Hz, while the apparent line widths were much larger at 300−400 Hz. In light of all this evidence, the β-spiral model of Urry represents only a subset of VPGVG-based elastic proteins. The Urry model misses the more populated distorted β-strand structure, which is likely a consequence of the use of a cyclic peptide in the model building and crystal structure determination.[9,11] The detection of the extended structure and an additional possible turn structure underscores the importance of quantitative distance and torsion angle measurements in structural studies. Chemical shifts alone do not have sufficiently high resolution to detect such structural heterogeneity. Our previous chemical shift analysis of elastin established one sufficient structural condition, which is the type II β-turn, and ruled out the ideal β-strands as possible conformations for elastin.[19] But it did not predict the distorted β-strand structure.

The type II β-turn and distorted β-strand conformations of $(VPGVG)_3$ have been detected in other VPGVG-like peptides using X-ray crystallography and solution NMR. For example, the crystal structure of Boc-VPGVG indicates a β-sheet conformation,[57] while solution NMR detected a β-turn structure for Boc-VPGVG-OMe.[58] Boc-VPGV was found to form two kinds of type II β-turn at the PG corner, with O−H distances of 2.13 and 2.18 Å.[59] These suggest that the VPGVG repeat sequence, notwithstanding variations in terminal protecting groups and sample preparation conditions, has an inherent preference for a β-sheet-like structure and a β-turn-like conformation.

The conformation distribution of $(VPGVG)_3$ sheds light on the mechanism of elasticity. The backbone intramolecular hydrogen bonds in the compact conformation would be disrupted upon stretching, thus shifting conformational equilibrium toward the distorted β-strand. Upon the release of the extension force, hydrogen bonds would re-form. Thus, interconversion between the two conformations would facilitate the elastic response of the protein. On the basis of our structure model (Figure 12), the length of each VPGVG unit, measured between V1 nitrogen and G5 carbonyl carbon, is $\sim$7 and $\sim$9 Å in the two compact structures but increases to $\sim$15 Å in the distorted β-strand structure. A similar conformational redistribution was also proposed for *Bombyx mori* silk fibroins, where the fraction of the β-turn structure decreases upon stretching while that of the β-sheet conformation increases with the stretching ratio.[60] Our proposed increase of the β-strand conformation in the stretched state of elastin implies that water is the key contributor to the elastomeric force. Since the distorted β-strand conformation has no backbone intramolecular hydrogen bonds, stretching should *increase* the conformational entropy of the polypeptide chain rather than decreasing it. Thus, the entropic elasticity would come from water−protein interactions. Indeed, molecular dynamics simulations on the pulling and releasing cycle of hydrated $(VPGVG)_{18}$ indicate that there are more backbone (ϕ, ψ) angle fluctuations in the extended state of the protein than in the relaxed state[55] and that water of hydrophobic hydration provides the main source of entropic elasticity.

Conclusion

We have determined the conformation of the central pentameric unit of the elastin-mimetic peptide $(VPGVG)_3$ using solid-state NMR. The peptide closely resembles the structure of $(VPGVG)_n$-based elastin according to ^{13}C and ^{15}N chemical shifts. Using site-specific labeled peptides, we determined two key distances across the PG residues and measured most of the (ϕ, ψ) torsion angles. The V6−V9 CO−H^N and CO−N distances indicate the coexistence of two types of conformations: one-third of the molecules adopt a compact structure with a short C−H distance of 3.3 ± 0.2 Å and a short C−N distance of 4.3 ± 0.2 Å, while two-thirds of the molecules have long C−H and C−N distances of about 7 Å. The compact structure is confirmed by a TEDOR-filtered C−H distance experiment and by dilution experiments that remove intermolecular couplings. The extended structure is confirmed by directly measured Pro and Gly ψ torsion angles, which are on average 150°. The structure distribution of PG residues is consistent with the G8 Cα CSA. For the other three residues of the repeat unit, the dominant (ϕ, ψ) angles correspond to the antiparallel β-strand conformation.

Conformational search of the Pro-Gly pair indicates that the compact structure is either a type II β-turn or a previously unclassified turn structure. The former has P7 torsion angles of ($-70°$, $120 \pm 20°$) and G8 torsion angles of ($80 \pm 20°$, $-20 \pm 20°$). The latter is characterized by P7 torsion angles of ($-70°$, $20 \pm 20°$) and Gly torsion angles of ($-100 \pm 20°$, $-20 \pm 20°$). The extended conformation is characterized by P7 ($-70°$, $160 \pm 5°$) and G8 ($-90 \pm 20°$, $\pm 158 \pm 5°$) and can be described as a distorted β-strand.

The conformation distribution of the PG pair in the VPGVG sequence may facilitate the extension/release cycle of the protein

(54) Debelle, L.; Alix, A. J. *Biochimie* **1999**, *81*, 981−994.
(55) Li, B.; Alonso, D. O. V.; Daggett, V. *J. Mol. Biol.* **2001**, *305*, 581−592.
(56) Asakura, T.; Ashida, J.; Ohgo, K. *Polym. J.* **2003**, *35*, 293.
(57) Ayato, H.; Tanaka, I.; Ashida, T. *J. Am. Chem. Soc.* **1981**, *103*, 5902−5905.
(58) Urry, D. W.; Cunningham, W. D.; Ohnishi, T. *Biochemistry* **1974**, *13*, 609−616.
(59) Yagi, Y.; Tanaka, I.; Yamane, T.; Ashida, T. *J. Am. Chem. Soc.* **1983**, *105*, 1242−1246.
(60) Asakura, T.; Yao, J. *Protein Sci.* **2002**, *11*, 2706−2713.

by shifting the conformational equilibrium. Upon extension, the protein would increase the fraction of the distorted β-strand conformation, which does not have backbone intramolecular hydrogen bonds. This lack of main-chain hydrogen bonds suggests an enhanced mobility or higher conformational entropy of the protein in the stretched state. This implies that the entropic elasticity should primarily result from the hydration water of the hydrophobic side chains rather than the conformational entropy of the polypeptide chains.

Acknowledgment. We thank D. Weliky for helpful discussions and V. P. Conticello for the poly(Lys-25) sample. M.H. gratefully acknowledges the Sloan Foundation for a research fellowship. This work is partially supported by the National Science Foundation (MCB-93398) and by the Research Corporation.

JA036686N